3D Reconstruction of Blood Vessel from Stereo X-ray Images

Qiuyu Chen

A thesis
submitted in partial fulfillment of the
requirements for the degree of

Master of Science in Electrical Engineering

University of Washington

2017

Committee:

Jeng-Neng Hwang, Chair

Linda Shapiro, Chair

Program Authorized to Offer Degree:
Electrical Engineering

University of Washington

Abstract

3D Reconstruction of Blood Vessel from Stereo X-ray Images

Qiuyu Chen

Co-Chairs of the Supervisory Committee:
Jeng-Neng Hwang

Linda Shapiro

We propose a fully automatic system to extract 3D structure of blood vessels from stereo X-ray images. Currently, typical 3D imaging technologies like angiography are expensive and potentially harmful to human body. In addition, for complex images with bones, 3D vessel representation will thus depend on further 3D tracing and segmentation. Because vessels are featureless and have low intensity contrast with background, other reconstruction methods like stereo are additionally challenging. Our system can effectively reconstruct main vessels in following steps. We first do initial segmentation using Markov Random Field and then further refine segmentation in an entropy based post-process. We then extract vessel centerlines and generate trees. Stereo matching is done in a coarse-to-fine scheme: Initial matching using affine transform and dense matching using Hungarian algorithm guided by Gaussian Regression [27]. We test and discuss its performance on stereo X-ray images and synthetic datasets. We also compare our method with human labeling and it achieves an accuracy of 71.08%.

ACKNOWLEDGMENTS

The author wishes to express sincere appreciation to University of Washington and National Institute of Informatics, where she has had the opportunity to work with Prof. Imari Sato,Prof. Jenq-Neng Hwang, Lin Gu, Bise Ryoma, Prof. Yinqiang Zheng. I am also very grateful to my parents' supports and love.

Chapter 1

INTRODUCTION

3D reconstruction of blood vessels has been widely studied recently in medical research. It allows practitioners to establish correct diagnosis and further reduce the threat of diseases like Cardiovascular and cancer [2, 24]. The current 3D vessel reconstruction techniques combines the means of acquisition and retrieval of the human body from different physical phenomenon such as computed tomography angiographic (CTA) images and magnetic resonance imaging (MRI). Angiography solves the reconstruction problem by limited number of projections under strong geometric assumptions on the blood vessels [20]. Perhaps the most related reconstruction method is point-based method. There are two types of approaches. One approach is based on stereo corresponding points which first manually identifies corresponding anatomical landmarks and then reconstructs with algorithms such as Direct Linear Transformation (DLT). The performance largely depends on the number of landmarks in the first step[13]. They are common accurate 3D imaging methods but the issue of high expense and high radiation dose become more essential. With less radiation harm, however, MRI are less accurate and more expensive [13]. In addition, These technologies usually require a long procedure time which may lead to the inaccuracy due to body deformation.

To reduce the cost, radiation and procedure time, we proposed a new system to obtain 3D reconstruction of blood vessels using only two stereo X-ray images. As shown in Fig1.a, stereo images are captured when x-ray light is fixed at position -a and +a. We are able to reconstruct blood vessels with X-ray position **a**, sample height **hs**, X-Ray height **hx**, and correspondence differences in two stereo images **d**. The process of calculating d is a stereo matching problem.

Stereo has been developed successfully in computer vision for many years [6, 26, 18].

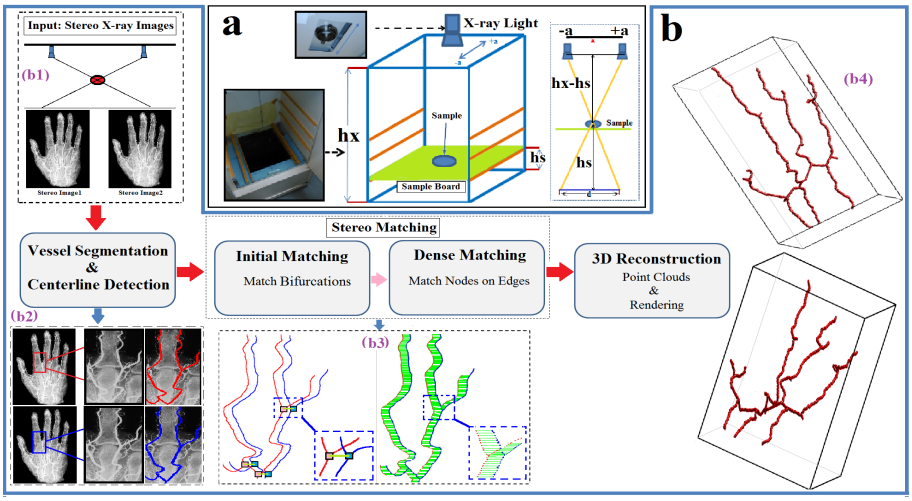

Figure 1.1: a. Equipment for Stereo X-ray Images. b. System workflow with examples for each steps

Generally, stereo matching methods can be categorized into pixel-based [4], window-based [30], feature-based [18, 16], and global optimization methods [5]. However, stereo matching remains difficult in textureless regions. This is also called the aperture problem [5]. For most of X-ray images, the intensity of vessel regions is featureless and low-contrast to background. It is not applicable in our context to do dense matching using traditional stereo methods based on intensity-consistency.

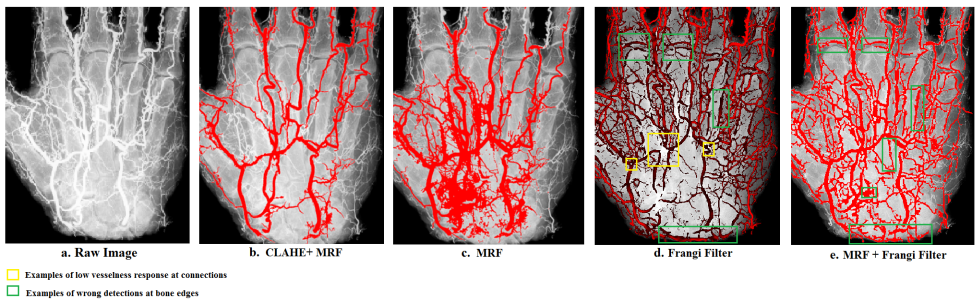

Figure 1.2: Segmentation Evaluation using Different Methods. a: raw image. b. Initial Segmentation using CLAHE and MRF. c: MRF. d:Frangi Filter e:MRF multi-label Optimization.

We are able to reconstruct vessels from bones in four main steps. After we get stereo X-ray images (Fig1. (b1)), we first do vessel segmentation, as shown in red and blue region in Fig1.(b2) and extract centerlines and tree for each stereo image. Stereo matching can be divided into initial matching and dense matching. During Initial matching (Fig1.(b3)-Left), we only match bifurcations using affine transform generated by SIFT on raw images. Dense matching uses Hungarian algorithm with Gaussian Regression [27] to assign each pair of correspondence along every edge linking between two matched bifurcations, as shown as green lines in Fig1.(b3)-Right. Using the correspondence differences in two stereo images, we can generate 3D point clouds and further get 3D rendering as shown in Fig1.(b4).

There are three main contributions of our work. First, we conduct a new system which can reconstruct blood vessels using two stereo images. It largely reduces patient's waiting time and radiation harm. Second, our method can particularly reconstruct vessels when they are mixed with bones. Third, our reconstruction method is accurate, it outperforms state-of-art dense stereo method and other point registration methods in our context.

This paper will be organized into the following sections: in section 2, we introduce details of vessel segmentation; section 3 talks about matching method and reconstruction steps; section 4 gives experiment results on stereo X-ray images and evaluate it's performance with human labeling of vessels in CT scan. We also give results on synthetic datasets. Finally, we conclude this work with a short discussion in section 5.

Chapter 2

VESSEL SEGMENTATION

Before reconstructing the 3D vessels, it is essential to segment and extract the vessel from input raw image as illustrated in Fig1.(b2). One of the widely used vessel segmentation method is proposed by Frangi *et.al.*[11] that measures the vesselness by computing the eigenvalues of Hessian at certain scale. The possibility of tubular structure is the maximum vesselness response across several selected scales which could be further determined by [19] using Markov random field(MRF). However, existing Frangi filter[11] and its combination with MRF method [19] suffer two limitations especially in current application: 1. Low vesselness response at vessel bifurcations where shapes are complex as illustrated in the yellow box in Fig2.d. 2. High vesselness response at background bone edge due to its high intensity illustrated in the green box in Fig2.d and Fig2.e.

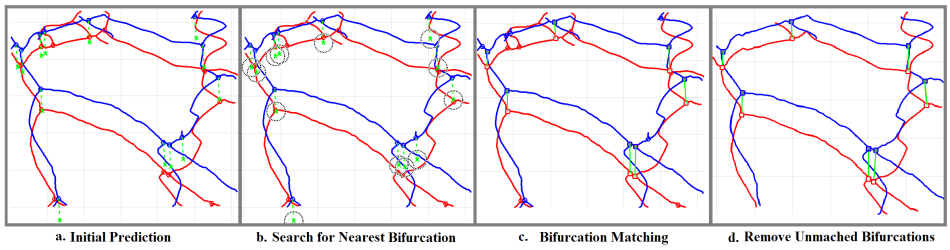

Figure 2.1: Stereo Matching Process. a. Initial prediction of corresponding bifurcation nodes using affine transform. b. Search for bifurcation nodes with minimum euclidean distance on targeted tree. Initial alignment.Blue dots represent warped image while red dots represent target image. c. Junction nodes matching. d. Remove branches with unmatched bifurcations

Since these two types of error would seriously spoil the preceding stereo matching and 3D reconstruction steps described in Sec.3, we apply a Contrast Limited Adapted Histogram Equalization(CLAHE)[33] method to enhance the vessel from complex background such as

high intensity bones. Adaptive Histogram Equalization(AHE) enhances the contrast between bones and vessels by amplifying the vicinity of each pixel by it's neighborhood cumulative distribution function (CDF). Since some noise may also be over amplified, CLAHE further limits the CDF by a threshold, to help equally redistribute among all histogram bins. Then we apply a MRF-optimization[14] to divide the enhanced image into several segmentations with labels. Based on the observation from raw image that vessel regions contribute slightly higher intensity, we look for pixels with high intensity and associate them with segmentation labels. The majority of labels in this set indicates the label of segmentation for vessel regions.

To further remove the noise such as bone edges and tiny vessels, we conduct series of entropy based morphological post-process. The vessel should show relative lower entropy because it is usually smoother than the bone. Therefore, we compute the local entropy on the raw image masked by initial segmentation and remove any pixel that has entropy higher than a threshold. This would also help us to remove thin vessels since vessel edges also have high entropy. We then only extract largest segmentation and fill holes through a morphological reconstruction algorithm [12]. Finally, fine vessel centerlines and trees are generated directly by [15] and [9].

Chapter 3

3D RECONSTRUCTION OF BLOOD VESSELS

3.1 Stereo Matching

Stereo Matching involves two steps: Initial Matching for bifurcations and Dense Matching for all the other nodes. Let **P** and **Q** represent bifurcation sets on warped image and target image, p_{i} and q_{i} represent bifurcation i on warped and target image.

3.1.1 Initial Matching:

In order to predict the correspondences on target image, we first calculate 3×3 affine transform using SIFT [18, 3] on the raw image. At each bifurcation (p_x, p_y) on warped image, we predict it's correspondence $(q\prime_x, q\prime_y)$ (Fig3.a). We use homogeneous coordinates to represent affine transform in a 3×3 matrix and homogeneous vector for each bifurcation pixel:

$$\begin{bmatrix} q\prime_x \\ q\prime_y \\ 1 \end{bmatrix} = \begin{bmatrix} \mathbf{R} & \mathbf{T} \\ \mathbf{0} & 1 \end{bmatrix} \begin{bmatrix} p_x \\ p_y \\ 1 \end{bmatrix} \tag{3.1}$$

where $\mathbf{R}$ is a 2×2 rotation matrix while $\mathbf{T}$ is a 2×1 translation vector. For each prediction, we then search for it's nearest bifurcation in $\mathbf{Q}$ within a range r (Fig3.b,c). We then remove edges between each unmatched bifurcation and it's connected terminal nodes (Fig3.d) and finally update trees for two images with N_J matched bifurcations.

3.1.2 Dense Matching:

The matched bifurcations suggest an initial mapping between two trees. A fine alignment approach using Hungarian algorithm guided by Gaussian Regression was proposed by [27]

to establish new matches between the edge points of the two paths. If we define the tree of warped image and targeted image as $\mathbf{X^A}$ and $\mathbf{X^B}$, then the correspondence set can be written as: $\pi = \{x_i^A \leftrightarrow x_i^B\}_{1 \leq i \leq N}$, N is the number of correspondence. Use Gaussian non-linear regression, we can predict the location of new correspondence of points in $\mathbf{X^A}$ by:

$$m_\pi(x^B) = \mathbf{k}^T \mathbf{C}_\pi^{-1} \mathbf{X}_\pi^A, \qquad \sigma^2(x^B) = k(x^B, x^B) + \beta^{-1} - \mathbf{k}^T \mathbf{C}_\pi^{-1} \mathbf{k}$$

where β is the measurement noise variance, k is a non-linear kernel function defined by Eq.2 and $\mathbf{C}_\pi$ is $N \times N$ matrix with element $C_{i,j} = k(x_i^B, x_j^B) + \beta^{-1}\delta_{i,j}$, $\mathbf{k}$ is the vector $[k(x_1^B, x^B), ..., k(x_N^B, x^B)]^T$

$$k(x_i, x_j) = \theta_0 + \theta_1 x_i^T x_j + \theta_2 exp\{-\frac{\theta_3}{2}\|x_i - x_j\|^2\} \tag{3.2}$$

We initialize the mapping using N_J sets of correspondences from initial matching: $\pi = \{p_i \leftrightarrow q_i\}_{1 \leq i \leq N_J}$. Following steps of fine alignment in [27], for each pair of edges connected by matched bifurcation, we find new correspondences and finally obtain dense matching.

3.2 Reconstruction

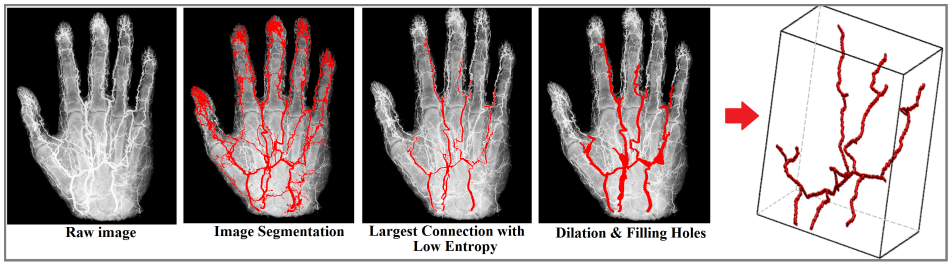

Figure 3.1: 3D reconstruction from stereo X-ray images of human hand

After we get correspondences: $\pi = \{x_i^A \leftrightarrow x_i^B\}_{1 \leq i \leq N}$, we estimate each point in world coordinate $\mathbf{X}_w^A$ and $\mathbf{X}_w^B$ using intrinsic matrix of the camera $\mathbf{M}$:

$$\mathbf{X}_w = \begin{bmatrix} x_w \\ y_w \\ 1 \end{bmatrix} = \mathbf{M}^{-1} \begin{bmatrix} x_i \\ y_i \\ 1 \end{bmatrix} \tag{3.3}$$

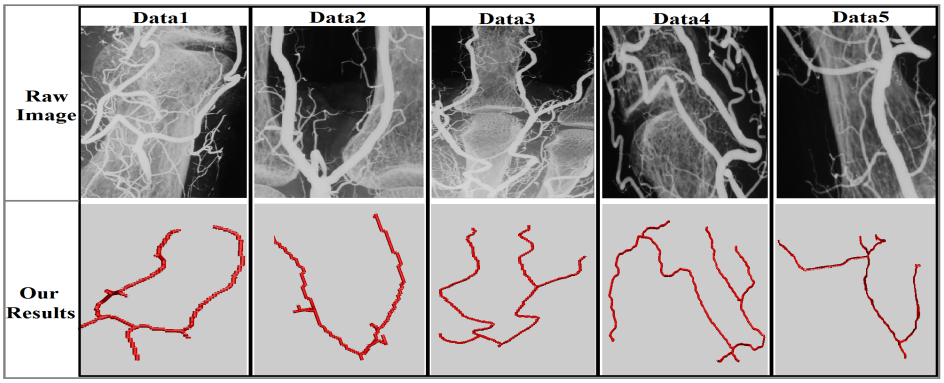

Figure 3.2: Experiments on 5 X-ray stereo images with bones. The first line shows 5 raw images, the second line shows their corresponding 3D rendering results using our method

As shown in Fig.1a, we assume X-ray light rail is parallel to image plane, if we define depth z as hx-hs, we can get Eq.4 based on similar triangles theorems:

$$\frac{2a}{d} = \frac{hx - hs}{hs} = \frac{z}{hx - z} \tag{3.4}$$

Since two X-ray lights are symmetric to the sample position, finally we estimate a 3D point $[x, y, z]^T$ as:

$$\begin{bmatrix} x \\ y \\ z \end{bmatrix} = \frac{1}{2} \times (\mathbf{X}_w^A + \mathbf{X}_w^B) + \begin{bmatrix} 0 \\ 0 \\ 2a \times \dfrac{hx}{d + 2a} - 1 \end{bmatrix} \tag{3.5}$$

We further smooth the reconstruction by averaging depth within a step size along each branch in the 3D tree. We assume blood vessels are cylinders with equal width, 3D rendering is done by applying a cylinder at each connection between two adjacent nodes in the tree. This step is done in Matlab trees Toolbox.

Chapter 4
EXPERIMENT

4.1 Experiment from X-ray Stereo Images

Our experiments are conducted in the equipment shown as Fig.1a with parameters of hx=100cm, hs=41cm and a=5cm. Fig.4 shows the whole reconstruction procedure on human hand from a pair of stereo X-ray images. After we get initial segmentation, we apply a 7×7 window to remove pixels with large local entropy. We also remove all the holes to avoid dead loops in tree structure, further do dilation to smooth vessel and remove noises and small branches. After stereo matching, we can generate point clouds and corresponding 3D models. In Fig.5, we also show reconstruction examples in details in 5 regions of a different hand.

4.2 Synthetic Experiment

We also design 4 synthetic vessel skeletons and render them as ground truth in Matlab Trees Toolbox. We simulate the experiment based on the principle of our equipment and project the 3D skeleton model into two stereo images. Because the projected stereo skeleton might be sparse, we further generate fine centerlines using morphological process. Using methods described in Section 3, we generate corresponding 3D models and compare them with ground truth.

4.3 Evaluation with Human Labeling

To evaluate the accuracy of point matching, we compare our results with CT scan. We simulate a projection of a stack of CT images on two stereo images. Due to high occlusion of bones and low resolution, we manually segment vessels and test accuracy of method in section 3. We associate our points with nearest human-labeled points on 2D CT image

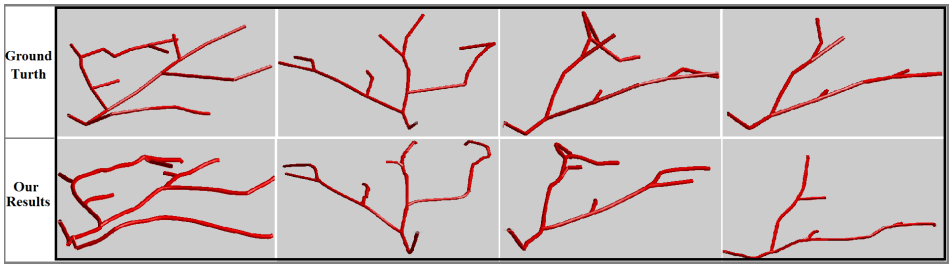

Figure 4.1: 4 examples of synthetic experiments

and evaluate each depth accuracy. We only care about the relative depth in this test so both CT and our results are normalized. We compare our results with state-of-art stereo matching method: Fullflow [7] and other non-rigid point matching methods: Coherent Point Drift (CPD) and Iterative Closest Point (ICP). We define error percentage for each point as $e\% = \frac{|Depth - GT|}{GT}$, and average accuracy is: $1 - \sqrt{\frac{\sum_{i=1}^{n} e_i^2}{n}}$, n is the number of points. As shown in Fig. 7, we achieve 72.6% points with less than 30% error, with an average accuracy of 71.8%. Fig.7b shows errors along blood vessels in 2D CT image. Typically, higher error may happen at vessel bifurcation, as shown in red squares. This is because when we generate centerline, there might be some displacement at bifurcations.

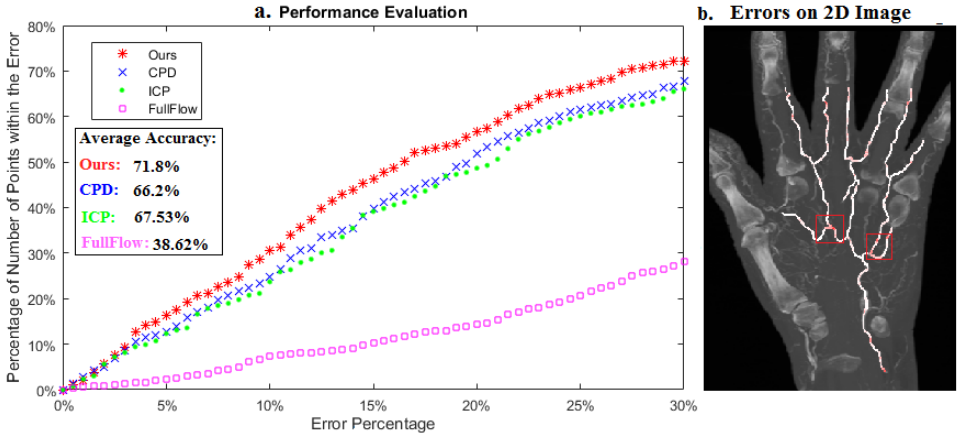

Figure 4.2: a. Accuracy Evaluations for our method, CPD and ICP and fullflow. b. Errors of our method shown on the 2D CT image.

Chapter 5

CONCLUSION

In this paper, we propose a system to reconstruct blood vessels from stereo X-ray images with bones. By evaluating our methods with human labeling and comparing with other methods, our method achieves higher accuracy. We would like to share our code and publish the dataset for research purpose.

BIBLIOGRAPHY

[1] Ali Al Moussawi, Cedric Galusinski, and Christian Nguyen. 3d reconstruction of blood vessels. *Engineering with Computers*, 31(4):775–790, 2015.

[2] et.al. Al Moussawi. 3d reconstruction of blood vessels. *Engineering with Computers*, 31(4):775–790, 2015.

[3] Marcel Berger. Geometry (vols. 1-2), 1987.

[4] S. Birchfield and C. Tomasi. A pixel dissimilarity measure that is insensitive to image sampling. *IEEE Transactions on Pattern Analysis and Machine Intelligence*, 20(4):401–406, Apr 1998.

[5] Y. Boykov, O. Veksler, and R. Zabih. Fast approximate energy minimization via graph cuts. In *Proceedings of the Seventh IEEE International Conference on Computer Vision*, volume 1, pages 377–384 vol.1, 1999.

[6] M. Z. Brown, D. Burschka, and G. D. Hager. Advances in computational stereo. *IEEE Transactions on Pattern Analysis and Machine Intelligence*, 25(8):993–1008, Aug 2003.

[7] Q. Chen and V. Koltun. Full flow: Optical flow estimation by global optimization over regular grids. In *2016 IEEE Conference on Computer Vision and Pattern Recognition (CVPR)*, pages 4706–4714, June 2016.

[8] Haili Chui and Anand Rangarajan. A new point matching algorithm for non-rigid registration. *Comput. Vis. Image Underst.*, 89(2-3):114–141, February 2003.

[9] Jaydeep De, Huiqi Li, and Li Cheng. Tracing retinal vessel trees by transductive inference. *BMC Bioinformatics*, 15(20):1–20, 2014.

[10] Martin A. Fischler and Robert C. Bolles. Random sample consensus: A paradigm for model fitting with applications to image analysis and automated cartography. *Commun. ACM*, 24(6):381–395, June 1981.

[11] Alejandro F. Frangi, Wiro J. Niessen, Koen L. Vincken, and Max A. Viergever. *Multiscale vessel enhancement filtering*, pages 130–137. Springer Berlin Heidelberg, Berlin, Heidelberg, 1998.

[12] Rafael C Gonzalez, Richard E Woods, and Steven L Eddins. Morphological reconstruction. *Digital Image Processing using MATLAB, MathWorks*, 2010.

[13] S Hosseinian and H Arefi. 3d reconstruction from multi-view medical x-ray images-review and evaluation of existing methods. *The International Archives of Photogrammetry, Remote Sensing and Spatial Information Sciences*, 40(1):319, 2015.

[14] Zoltan Kato and Ting-Chuen Pong. *A Markov Random Field Image Segmentation Model Using Combined Color and Texture Features*, pages 547–554. Springer Berlin Heidelberg, Berlin, Heidelberg, 2001.

[15] L. Lam, S. W. Lee, and C. Y. Suen. Thinning methodologies-a comprehensive survey. *IEEE Transactions on Pattern Analysis and Machine Intelligence*, 14(9):869–885, Sep 1992.

[16] C. Liu, J. Yuen, and A. Torralba. Sift flow: Dense correspondence across scenes and its applications. *IEEE Transactions on Pattern Analysis and Machine Intelligence*, 33(5):978–994, May 2011.

[17] X. Liu, M. Song, D. Tao, Z. Liu, L. Zhang, C. Chen, and J. Bu. Random forest construction with robust semisupervised node splitting. *IEEE Transactions on Image Processing*, 24(1):471–483, Jan 2015.

[18] D. G. Lowe. Object recognition from local scale-invariant features. In *Proceedings of the Seventh IEEE International Conference on Computer Vision*, volume 2, pages 1150–1157 vol.2, 1999.

[19] H. Mirzaalian and G. Hamarneh. Vessel scale-selection using mrf optimization. In *2010 IEEE Computer Society Conference on Computer Vision and Pattern Recognition*, pages 3273–3279, June 2010.

[20] D. Mitton, C. Landry, S. Véron, W. Skalli, F. Lavaste, and J. A. De Guise. 3d reconstruction method from biplanar radiography using non-stereocorresponding points and elastic deformable meshes. *Medical and Biological Engineering and Computing*, 38(2):133–139, 2000.

[21] Francesc Moreno-Noguer, Vincent Lepetit, and Pascal Fua. *Pose Priors for Simultaneously Solving Alignment and Correspondence*, pages 405–418. Springer Berlin Heidelberg, Berlin, Heidelberg, 2008.

[22] James R. Munkres. Algorithms for the Assignment and Transportation Problems. *Journal of the Society for Industrial and Applied Mathematics*, 5(1):32–38, March 1957.

[23] A. Myronenko and X. Song. Point set registration: Coherent point drift. *IEEE Transactions on Pattern Analysis and Machine Intelligence*, 32(12):2262–2275, Dec 2010.

[24] H. Qin and Z. Li. Three dimentional reconstruction of blood vessels and evaluation of vascular stenosis based on dsa. In *International Conference on Advanced Materials and computer science*, 2016.

[25] H. Qin and Z. Li. Three dimentional reconstruction of blood vessels and evaluation of vascular stenosis based on dsa. In *International Conference on Advanced Materials and computer science*, 2016.

[26] Daniel Scharstein and Richard Szeliski. A taxonomy and evaluation of dense two-frame stereo correspondence algorithms. *International Journal of Computer Vision*, 47(1):7–42, 2002.

[27] E. Serradell, M. A. Pinheiro, R. Sznitman, J. Kybic, F. Moreno-Noguer, and P. Fua. Non-rigid graph registration using active testing search. *IEEE Transactions on Pattern Analysis and Machine Intelligence*, 37(3):625–638, March 2015.

[28] Burr Settles. Active learning literature survey. Technical report, 2010.

[29] Jian Sun, Nan-Ning Zheng, and Heung-Yeung Shum. Stereo matching using belief propagation. *IEEE Transactions on Pattern Analysis and Machine Intelligence*, 25(7):787–800, July 2003.

[30] Ramin Zabih and John Woodfill. *Non-parametric local transforms for computing visual correspondence*, pages 151–158. Springer Berlin Heidelberg, Berlin, Heidelberg, 1994.

[31] X. Zhu, C. C. Loy, and S. Gong. Constructing robust affinity graphs for spectral clustering. In *2014 IEEE Conference on Computer Vision and Pattern Recognition*, pages 1450–1457, June 2014.

[32] Xiaojin Zhu. Semi-supervised learning literature survey. 2006.

[33] Karel Zuiderveld. Graphics gems iv. chapter Contrast Limited Adaptive Histogram Equalization, pages 474–485. Academic Press Professional, Inc., San Diego, CA, USA, 1994.